Endothelial cell polarization and chemotaxis in a microfluidic device†

Amir Shamloo,[a] Ning Ma,[b] Mu-ming Poo,[c] Lydia L. Sohn[b] and Sarah C. Heilshorn*[d]

Received 4th January 2008, Accepted 12th May 2008
First published as an Advance Article on the web 30th May 2008
DOI: 10.1039/b719788h

The directed migration of endothelial cells is an early and critical step in angiogenesis, or new blood vessel formation. In this study, the polarization and chemotaxis of human umbilical vein endothelial cells (HUVEC) in response to quantified gradients of vascular endothelial growth factor (VEGF) were examined. To accomplish this, a microfluidic device was designed and fabricated to generate stable concentration gradients of biomolecules in a cell culture chamber while minimizing the fluid shear stress experienced by the cells. Finite element simulation of the device geometry produced excellent agreement with the observed VEGF concentration distribution, which was found to be stable across multiple hours. This device is expected to have wide applicability in the study of shear-sensitive cells such as HUVEC and non-adherent cell types as well as in the study of migration through three-dimensional matrices. HUVEC were observed to chemotax towards higher VEGF concentrations across the entire range of concentrations studied (18–32 ng mL^{-1}) when the concentration gradient was 14 ng mL^{-1} mm^{-1}. In contrast, shallow gradients (2 ng mL^{-1} mm^{-1}) across the same concentration range were unable to induce HUVEC chemotaxis. Furthermore, while all HUVEC exposed to elevated VEGF levels (both in steep and shallow gradients) displayed an increased number of filopodia, only chemotaxing HUVEC displayed an asymmetric distribution of filopodia, with enhanced numbers of protrusions present along the leading edge. These results suggest a two-part requirement to induce VEGF chemotaxis: the VEGF absolute concentration enhances the total number of filopodia extended while the VEGF gradient steepness induces filopodia localization, cell polarization, and subsequent directed migration.

Introduction

Mammalian cell culture is an important and common tool in modern biology. Microfluidic devices can be very helpful as platforms for mammalian cell culture because they allow control over the local microenvironment and greatly reduce the volume of costly reagents required.[1,2] Therefore, microfluidic devices are particularly well-suited to study the effects of concentration gradients on cell cultures. Early microfluidic concentration gradient generators used serpentine inlet channels to create a stable concentration gradient in a cell culture environment.[3] These microdevices have been used to study the differentiation of neuronal stem cells[4] and the migration of neutrophil cells subjected to a growth factor concentration gradient.[5] However this design requires fluid convection through the cell culture chamber, which can be a confounding factor in many cell culture systems. For example, endothelial cells, which line the cardiovascular system, will align parallel to the direction of fluid flow, making it impossible to study chemotactic migration in these microdevices without the orthogonal influence of shear stress.[6] Similarly, non-adherent cultures, such as embryoid bodies of stem cells, cannot be studied in microdevices with continuous flow. Furthermore, the presence of continuous flow can induce directed migration even in cell types not normally considered to be shear sensitive.[7] An additional limitation of continuous flow devices is that they are unable to study cell migration through three-dimensional substrates.

Responding to these limitations, several groups have designed microfluidic devices that rely solely on diffusion to produce concentration gradients for various biological applications.[8–16] These devices have been used to study bacterial[8,9] and neutrophil[10,14,15] chemotaxis. In general, these devices either require additional fabrication steps to add membranes or hydrogels into the device, are limited to small cell culture areas that limit cell migration to one-dimension, or are unable to maintain equilibrium concentration gradients for long-term culture. Therefore, our goal is to design a simple microdevice geometry that is capable of producing a stable concentration gradient while minimizing fluid convection inside the cell chamber in order to study endothelial cell migration.

Endothelial cell motility plays an important role in many biological processes, including wound healing[17] and cancer development.[18] In these phenomena, angiogenesis, the formation of new blood vessels, is required to supply nutrients to

[a]*Department of Mechanical Engineering, Stanford University, Stanford, CA, USA*
[b]*Department of Mechanical Engineering, University of California, Berkeley, Berkeley, CA, USA*
[c]*Department of Molecular and Cell Biology, University of California, Berkeley, Berkeley, CA, USA*
[d]*Department of Materials Science and Engineering, Stanford University, Stanford, CA, USA. E-mail: heilshorn@stanford.edu*
† Electronic supplementary information (ESI) available: Fig. S1–S4. See DOI: 10.1039/b719788h

the developing tissue. An early and critical step in angiogenesis is the migration of endothelial cells away from existing blood vessels and into the surrounding tissue.[19] Tissue engineering and regenerative medicine therapies are also dependent upon endothelial cell migration, as regenerated tissue requires vascularization for survival.[19] During endothelial cell migration, cells may respond to several environmental cues that activate different types of receptors. These cues include shear stress induced by fluid motion,[6] soluble growth factors,[20] and substrate-bound ligands.[21] Studying each of these migration factors independently and quantitatively is a critical first step towards analyzing the role of different cell migration mechanisms and the potential crosstalk between these systems.[22–24]

It has been hypothesized that gradients of vascular endothelial growth factor (VEGF) carried by interstitial flow brings about the formation of long capillary structures *in vivo*.[25,26] Delivery of exogenous VEGF is also being explored as a therapeutic factor to induce angiogenesis in ischemic tissue.[27,28] The migration of human umbilical vein endothelial cells (HUVEC) is a well studied *in vitro* model of VEGF chemotaxis in the absence of shear stress. Shear-free chemotaxis is generally studied using protocols that generate concentration gradients that continuously change over time, making quantification and long-term studies difficult (*e.g.*, transwell inserts,[29] Boyden chambers,[30] and Zigmond and Dunn chambers[31,32]). Furthermore, the short half-life of VEGF under standard cell culture conditions (~50 min)[33] requires constant replenishment for quantitative long-term studies. Therefore, we propose a simple device to quantitatively study polarization and chemotaxis of shear-sensitive mammalian cells using stable, quantifiable concentration gradients of growth factors that are constantly replenished. In this device, the steady-state diffusion of guidance cues across the cell culture chamber creates the concentration gradient while fluid convection is minimized. The device is composed of two reagent channels (the source and sink channels), which convey the fluid, and a cell culture chamber positioned between these two reagent channels, Fig. 1. The cell culture chamber and the reagent channels are connected using microcapillaries in order to allow Fickian diffusion of guidance cues from the source channel through the cell culture chamber and into the sink channel. Because the microcapillaries inhibit fluid convection into the cell culture chamber, the cells experience minimal shear stress. This simple design provides the opportunity to analyze HUVEC polarization and chemotaxis in response to a constant, quantifiable concentration gradient of VEGF independent from the effects of physiological fluid shear stress.

In this device, HUVEC showed migration toward higher concentrations of VEGF when subjected to a 14 ng mL^{-1} mm^{-1} gradient for 6 h. However, HUVEC exposed to a shallower 2 ng mL^{-1} mm^{-1} VEGF gradient at similar absolute concentrations were not observed to chemotax. Interestingly, the increased formation of filopodia along the leading edge of chemotaxing cells was also observed in the steeper VEGF concentration gradients, showing an active migrating mechanism in the cytoskeleton of these cells. In contrast, HUVEC exposed to high VEGF absolute concentrations in shallow gradients displayed increased numbers of filopodia uniformly distributed around the entire cell perimeter. Taken together, these results suggest that a change in VEGF concentration across the surface of a single cell

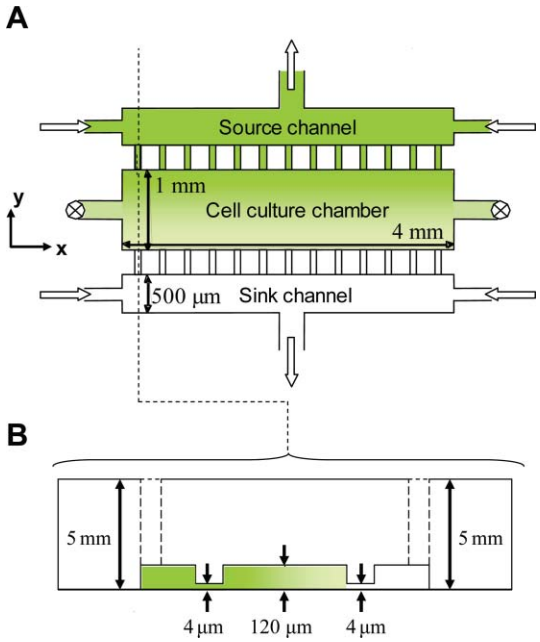

Fig. 1 Schematic of microfluidic device. (A) Top view, showing positions of source and sink (reagent) channels and cell culture chamber. The microcapillaries (5 μm width repeated every 15 μm, not drawn to scale) connect the reagent channels to the cell culture chamber. (B) Cross-section view of the device showing the thickness of each layer. The dashed lines show positions of the inlets and outlets at both ends.

(rather than the absolute VEGF concentration) stimulates the localization of VEGF-induced filopodia, resulting in cell polarization. The direction of cell polarization positively correlates with the direction of chemotactic migration. This study suggests a two-part requirement to induce VEGF chemotaxis: the VEGF absolute concentration enhances the total number of filopodia extended while the VEGF gradient steepness induces filopodia localization and cell polarization.

Materials and methods

Microfluidic device simulation

A finite element model (Comsol, Stockholm, Sweden) was generated to simulate fluid flow and reagent diffusion in the device. The steady-state Navier–Stokes equation was solved to obtain the flow field, and the transient convection–diffusion equation was solved to obtain the concentration distribution of reagents in the microfluidic channels. In order to ensure that the results are independent from the spatial discretization, the finite element mesh was coarsened and refined by a factor of two and the simulation was repeated.

Microfluidic device fabrication

The microfluidic chamber was fabricated using standard soft lithography and micromolding techniques at the Stanford Microfluidics Foundry clean room. A transparency mask was printed using a high-resolution printer (Fineline Imaging, Colorado Springs, CO). Fabrication of master molds was performed by patterning two layers of negative SU8 photoresist (MicroChem, Newton, MA) on a silicon wafer (layer 1: SU8–5,

~4 μm; layer 2: SU8-100, ~120 μm). The mold was coated with chlorotrimethylsilane (Sigma) to allow easy removal of the polymeric replica. The replica was fabricated using PDMS (Sylgard 184, Midland, MI) micromolding against the master mold. Sharpened needles (20 gauge) were used to punch inlets and outlets to the cell culture chamber and reagent channels. Both the surfaces of glass and PDMS were treated with plasma cleaner and brought together to bond irreversibly.

Concentration gradient generation

Tubings (Upchurch Scientific, Oak Harbor, WA) were inserted into the inlet holes of the device and connected to 100 μL syringes (Hamilton, Reno, NV) mounted on a syringe pump (World Prerecision Instruments, Sarasota, FL). Verification of the reagent concentration distribution was performed using digital imaging of a fluorescent biomarker which is similar in size to VEGF protein, FITC-Dextran (MW = 20 kDa, Sigma). The images for concentration distribution were taken using a fluorescent inverted microscope (Zeiss, Oberkochen, Germany) with a CCD camera and analyzed using Matlab for flow rates ranging from 2–60 nL min^{-1}. To measure the fractional concentration at each position in the cell culture chamber, fluorescence intensity of each image pixel was measured and normalized to the intensity of the solution injected in the source channel which has the same height as the cell culture chamber. Control experiments showed the fluorescence intensity was linearly related to concentration across the range of variables tested in these studies.

Cell preparation

Human umbilical vein endothelial cells (HUVEC, Lonza, Walkersville, MD) were grown in Endothelial Growth Medium-2 (EGM-2, 2% serum, Lonza). The media was changed every two days, and cells were kept in a humidified, 5% CO_2 environment at 37 °C. HUVEC were passaged non-enzymatically using EDTA solution (Gibco, Grand Island, NY). Passages 2–7 were used for each experiment, and the behaviour of cells remained the same during these passages.

Cell viability

Prior to cell seeding, devices were autoclaved. Fibronectin solution (10 μg mL^{-1}, Sigma) was injected into the cell culture chamber, incubated overnight, and rinsed twice with phosphate buffered saline (PBS). Suspended HUVEC (600 000 cells mL^{-1}, EGM-2) were injected into the cell culture chamber and plug-pins were used to close the injection ports of the chamber. The surface of the device was covered with sterile wet gauze to regulate humidity. Cell viability was assessed by injecting trypan blue (Gibco) to label dead cells. Control cultures were grown in standard tissue culture petri dishes coated with fibronectin as described above (Falcon). Three independent experiments were performed.

Cell chemotaxis

Suspended HUVEC were injected into the device as above. After 20 min incubation, HUVEC were observed to adhere to the substrate and their original positions were imaged using a phase-contrast inverted microscope (this is designated as $t = 0$). Media containing VEGF-A isoform VEGF(165) (50 ng mL^{-1}, R&D Systems, Minneapolis, MN; hereafter referred to as simply VEGF) was injected into both inlets of the source channel. In the sink channel, media without VEGF was injected. The injection rate was 8 nL min^{-1}, which was shown to give a stable concentration gradient along the cell culture chamber.

After 6 h, the device was again imaged to determine final cell positions. The cell culture chamber was divided into four equal zones transversely. By counting the number of cells in each zone at $t = 0$ and 6 h, the net change in the number of cells was determined. Three to five independent experiments were performed at each condition.

Fluorescence microscopy

Cells were rinsed several times by injecting PBS into the cell culture chamber, fixed with 4% paraformaldehyde in PBS for 15 min at room temperature, rinsed twice with PBS, and blocked with normal goat serum for 2 h. Rhodamine–phalloidin (Molecular Probes) was injected into the chamber and allowed to incubate in the dark for 1 h. The chamber was thoroughly rinsed twice with PBS for 5 min. Next, 6-diamidino-2-phenylindole (3×10^{-7} M, DAPI, Molecular Probes) was added into the cell chamber and incubated for 5 min in the dark. Finally, the cells were rinsed with PBS three times and fluorescently imaged using the inverted microscope. ImageJ software (NIH freeware) was used to find the center of mass for each cell to determine the centerline bisecting the cell perpendicular to the gradient direction. The total number of filopodia (extensions with length >3 μm and width <1 μm) for each cell, the number of filopodia located on the cell side oriented toward the higher concentration of VEGF, and the number of filopodia located on the cell side oriented toward the lower concentration of VEGF were determined.

Statistical analysis

Average and standard deviation of the experimental results are reported. One-tailed, non-paired student T-test was used to determine the significance of differences between the net change in the number of the cells in migration zones and also the number of filopodia in chemotaxing and non-chemotaxing cells.

Results and discussion

Design and simulation of microfluidic device

The two goals of our microfluidic device design are (1) to create a stable concentration gradient and (2) to minimize fluid convection within the cell culture chamber. A finite element simulation of the device was created to test various design parameters. In order for the device to be at equilibrium, the flow rate through the reagent channels must be fast enough to replenish the source channel with fresh guidance cue and sweep away guidance cue immediately after reaching the sink channel. Therefore, the appropriate flow rate to give a uniform concentration gradient will be dependent on the diffusivity of the guidance cue. As VEGF is a protein with low diffusivity ($D = 9.4 \times 10^{-7}$ cm^2 s^{-1}),[34] the flow required to maintain equilibrium

should be rather slow, so that the diffusion time of VEGF molecules into the cell chamber is comparable with the VEGF residence time as it is carried through the reagent channels. To predict the optimum convection time for VEGF, finite element simulations were run with injection rates from 2–60 nL min^{-1}. At the optimum flow rate of 8 nL min^{-1}, the concentration gradient profile is stable along the entire *x*-axis of the cell culture chamber, Fig. 2A. At this flow rate, the VEGF concentration gradient within the cell culture chamber is predicted to be 26% of the source concentration per mm, with minimum and maximum concentrations of 37% and 63%, respectively.

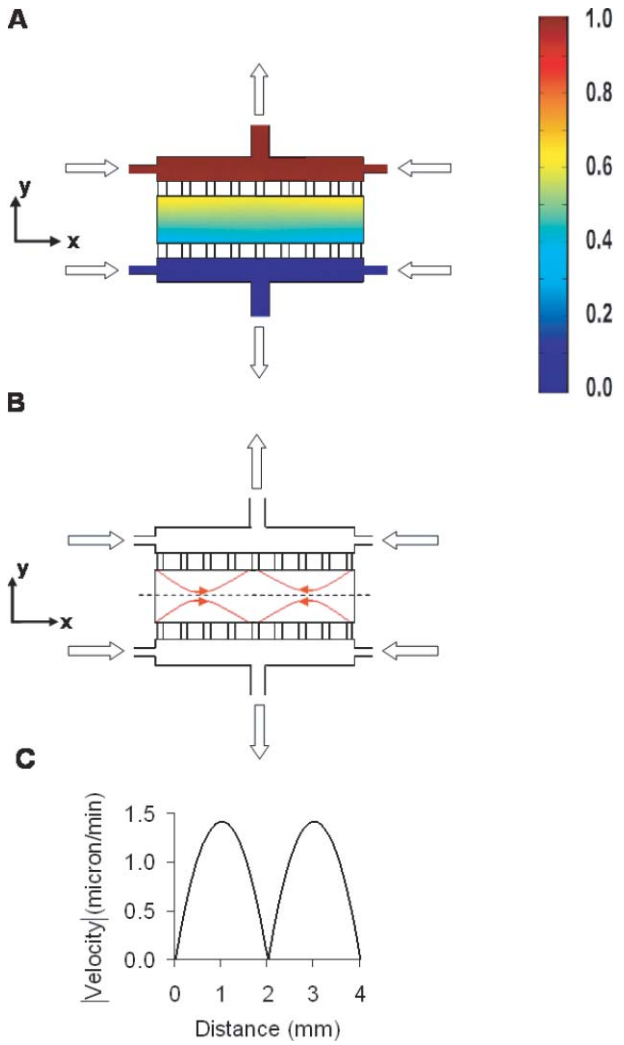

Fig. 2 Simulation results for the microfluidic device. (A) The concentration gradient generated in the cell culture chamber at an injection flow rate of 8 nL min^{-1}. The normalized scale runs from 100% (1.0, red) of the source concentration to 0% (0.0, blue) at the sink. (B) Fluid flow streamlines showing the cross-current flow pattern in the cell culture chamber produced due to the pressure drop between inlets and outlets. (C) Absolute value of fluid velocity along the dashed line shown in B, where the predicted maximum fluid velocity within the cell culture chamber occurs assuming equal inlet flow rates.

Next, the finite element simulation was used to analyze the flow profile throughout the device. The maximum fluid speed within the cell culture chamber was predicted to occur along the centerline of the device ($y = 0.5$ mm), Fig. 2B, assuming equal inlet flow rates in the source and sink channels. (Predicted streamlines in the sink and source channels have been removed to highlight the streamlines in the cell culture chamber; see ESI† for the full Comsol simulation.) Along this centerline, the predicted maximum fluid speed occurred midway between the channel inlets and outlets ($x = 1$, 3 mm). At all locations within the device, the absolute value of fluid velocity was below 1.5 μm min^{-1}, Fig. 2C. Using this result, it is possible to approximate the maximum shear stress experienced by cells in the cell culture chamber. The maximum shear stress value for a hemispherical cell located in a laminar flow can be estimated as:

$$\tau = \frac{3\mu U}{2a}$$

where U is the fluid velocity, μ is the fluid viscosity, and a is the average diameter of the endothelial cells.[35] Using this estimation, the maximum shear stress in the cell culture chamber is ~10^{-5} dyn cm^{-2} for the injection rate used in our experiments (8 nL min^{-1}). This value is much below the physiological shear stress applied to endothelial cells in blood vessels (~12 dyn cm^{-2}) and also below the shear stress range that can induce cell alignment (~3 dyn cm^{-2}).[23]

Quantification of the concentration gradient

To quantitatively analyze the concentration gradient of biomolecules in the cell culture chamber, a fluorescent biomarker was chosen with molecular weight and diffusivity similar to VEGF (5 μM FITC–Dextran, MW = 20 kDa; VEGF MW~20 kDa; D~9.4 × 10^{-7} cm^2 s^{-1}).[34] The concentration distribution of FITC–Dextran was measured in the middle and at the ends of the cell culture chamber ($x = 0$, 2, and 4 mm), Fig. 3A. The width of the selected zones for data analysis was about 1% of the total channel length, Fig. 3B. In order to create a stable and uniform concentration gradient along the *x*-axis of the cell culture chamber, different injection flow rates were tested from 2 to 60 nL min^{-1}. Similar to the simulation results, an injection flow rate of 8 nL min^{-1} was shown to generate stable concentration profiles at the selected inlet and outlet zones, Fig. 3C. At this flow rate, the device required 45 min to fully develop an equilibrium concentration gradient that then remained unchanged during the duration of a typical 6 h experiment (see ESI†). These experimental results showed excellent comparison with the predicted simulation values. Based on these results, a flow rate of 8 nL min^{-1} was chosen for all subsequent experiments.

Similar linear concentration gradients were obtained when the cell culture chamber was filled with three-dimensional hydrogel matrix (data not shown). Therefore, the device geometry creates a large culture surface (1 mm × 4 mm) with a fully predictable and stable concentration distribution across the entire culture chamber. Furthermore, the concentration gradients at the device inlets and outlets were indistinguishable from one another using fluorescent quantification, which ensures that cells throughout the device experience a similar microenvironment. This has been a confounding factor in experiments using continuous flow gradient generators, where the gradient steepness continuously declines across the *x*-axis of the device.[7,36] Compared to other equilibrium, diffusion-based gradient generators, this

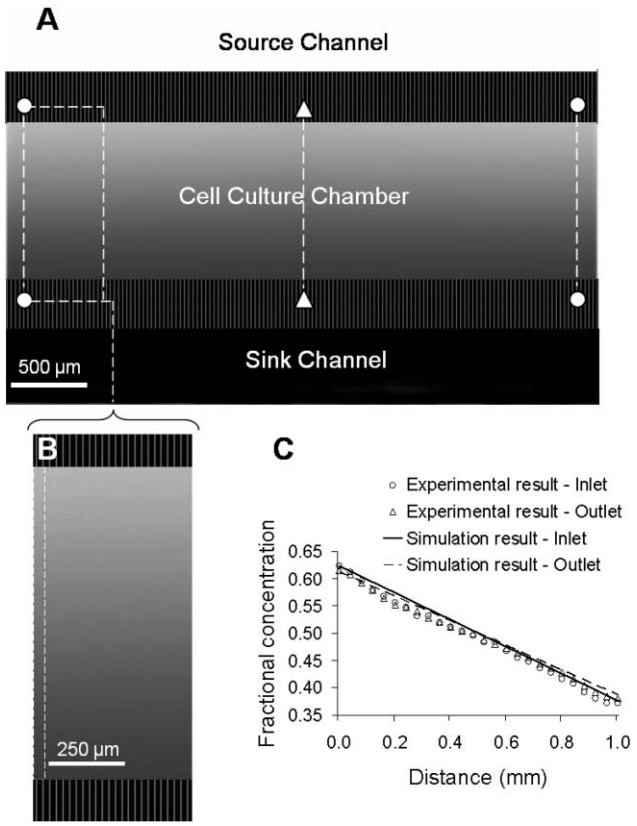

Fig. 3 Concentration gradient profile in the cell culture chamber. (A) FITC–dextran concentration gradient generated in the cell culture chamber at an injection flow rate of 8 nL min^{-1}. Circles and triangles depict the locations where simulation and experimental results were compared. (B) Representative fluorescent image of the concentration gradient in the inlet region. The pixel intensity of the concentration distribution is averaged over the area shown with a dashed line. (C) Concentration gradient as a fraction of the source concentration at the inlets (circle = experimental observation, solid line = simulation) and outlets (triangle = observation, dashed line = simulation) at a flow rate of 8 nL min^{-1}.

device provides a large cell culture surface and is fabricated using a single-layer PDMS mold without requiring additional membrane, filter, or hydrogel components. This simple design is expected to be widely applicable to the study of cell polarization and chemotaxis in both two- and three-dimensions of multiple cell types, including those that are non-adherent or shear sensitive.

Viability of HUVEC

HUVEC were monitored over 3 days in devices both with and without fluid flow. In both cases, EGM-2 media without supplemental VEGF was used. Viability within the device with flow was comparable to HUVEC viability cultured in standard petri dishes (~90%, see ESI†). As expected, the results showed an increase in viability in the presence of fluid flow in the reagent channels. This is presumably due to the diffusion of nutrients into the culture chamber as fresh media is injected into the reagent channels. At no time point did the cells in the culture chamber appear to align along the putative cross-current flow patterns (data not shown). This confirms that our designed device enables the study of HUVEC polarization and chemotaxis in the absence of shear-induced alignment.

HUVEC chemotaxis in stable VEGF gradients

To study HUVEC migration in response to VEGF concentration gradients, media containing 50 ng mL^{-1} of VEGF was injected into the source channel at 8 nL min^{-1} resulting in a gradient of 14 ng mL^{-1} mm^{-1} along the *y*-axis of the cell culture chamber and an average absolute concentration of 25 ng mL^{-1}. The maximum concentration in the cell culture chamber (32 ng mL^{-1}) was chosen to be below the reported VEGF receptor saturation level for human dermal microvascular cells (40–100 ng mL^{-1}).[33] HUVEC distribution in the cell culture chamber was imaged before and after 6 h of gradient exposure, Fig. 4A, B. The cell culture chamber was divided into four equal zones transversely, in order to determine the distribution of cells before and after chemotaxis. The width of these zones (250 μm) was chosen in order to be large enough to coarsen the effects of random cell seeding and produce a uniform initial cell distribution while being small enough to allow monitoring of migration at multiple regions across the *y*-axis of the chamber.

About 7% of HUVEC originally in zone 1 (with the lowest VEGF concentration) were found to migrate into zones with higher VEGF concentrations, Fig. 4C. (Note, cells are unable to enter the microcapillaries that flank the cell culture chamber.) Similarly, an increase in cell number of ~11% was found in zone 4 (the highest VEGF concentration) after exposure to the gradient. Accordingly, the numbers of cells found in zones 2 and 3 were relatively unchanged during the experiment. This suggests that approximately equal numbers of cells entered into and departed each of these zones. Therefore, across the range of absolute concentrations tested (18–32 ng mL^{-1}), HUVEC chemotaxis remained relatively uniform, suggesting a wide range of VEGF concentrations is capable of initiating chemotaxis. As a negative control, the experiment was repeated using basal medium (no VEGF supplementation) in both the source and sink reagent channels. In the absence of a VEGF gradient, the HUVEC distribution remained random throughout the device (see ESI†).

In the above experiments, HUVEC were allowed to adhere for 20 min on the fibronectin substrate prior to the onset of VEGF gradient exposure (noted as $t = 0$ h). To ensure that HUVEC motility was not artificially enhanced by the short culture time, this experiment was repeated after HUVEC were given 24 h to firmly adhere to the fibronectin substrate and form strong focal adhesion sites with the matrix. Similar to the previous results, about ~6% of HUVEC originally in zone 1 were found to migrate into zones with higher VEGF concentrations, the number of cells in zones 2 and 3 remained unchanged, and an increase in cell number of ~7% was found in zone 4, Fig. 4D. These results suggest that a 20 min adhesion time is sufficient for HUVEC to adhere firmly to the fibronectin substrate. HUVEC adhesion to fibronectin is mediated through multiple cell-binding domains that are recognized by cell-surface integrin receptors. Integrins are heterodimeric transmembrane proteins that mediate both cell adhesion and migration. Multiple integrin receptors have been implicated in angiogenesis,[37,38] and VEGF is known to activate at least one fibronectin integrin, $\alpha_5\beta_1$, to enhance HUVEC adhesion and migration on fibronectin.[37]

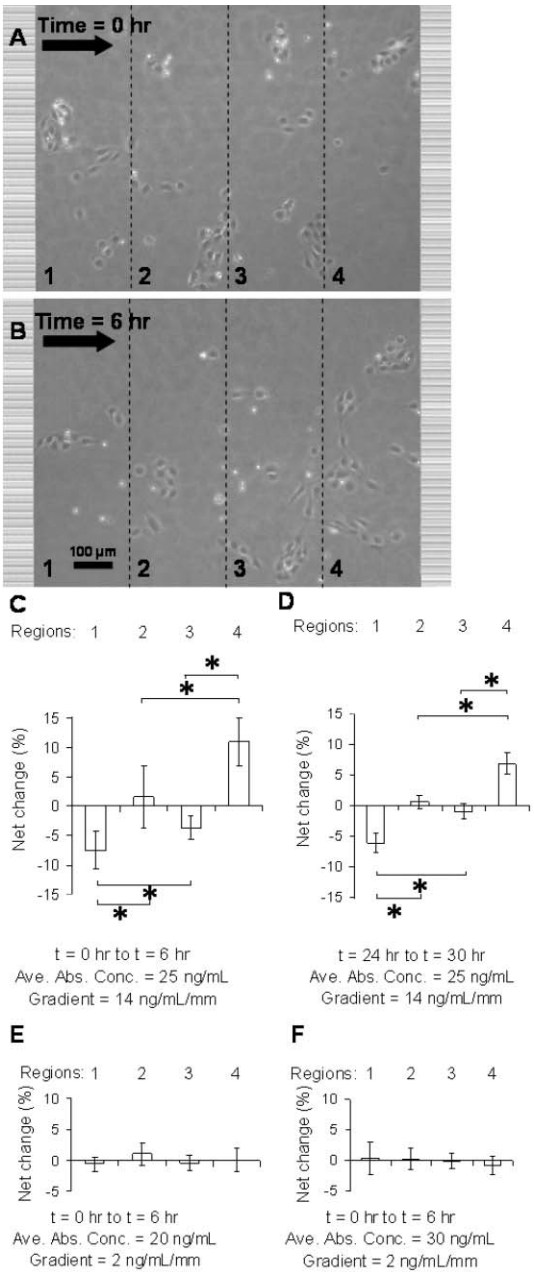

Fig. 4 HUVEC chemotaxis in the cell culture chamber. (A, B) Representative phase contrast images of cell positions at time = 0, 6 h during chemotaxis (gradient = 14 ng mL^{-1} mm^{-1}, average absolute concentration = 25 ng mL^{-1}). The cell culture chamber is divided into four equal zones transversely in order to determine the distribution of the cells before and after migration. The arrow points toward higher VEGF concentrations. (C–F) The net change in the number of cells within each zone under various concentration conditions. Data represent averages of $n = 3$–5 independent experiments ± standard deviation. *Statistically significant, $p < 0.05$.

VEGF activation of multiple integrin heterodimers is mediated by the VEGFR2 receptor via a PI3-kinase signalling pathway that can also enhance HUVEC migration on other extracellular matrix substrates such as vitronectin and type I collagen.[37] Our simplified model of HUVEC chemotaxis on fibronectin takes a reductionist approach to begin to quantitatively elucidate the requirements for VEGF-induced chemotaxis. In future studies, complexity can be systematically introduced into the model (for example, by testing various ligand densities[23,37] and mixtures of matrix substrates to more accurately reflect the *in vivo* environment) to determine the quantitative effects on VEGF-mediated chemotaxis.

Previous results have demonstrated that a minimum VEGF gradient >25 ng mL^{-1} mm^{-1} is required to induce alignment of three-dimensional endothelial cell sprouting with an absolute concentration of 100 ng mL^{-1}.[33] To determine if a similar threshold gradient response is required to induce two-dimensional HUVEC polarization and chemotaxis, we reduced the concentration gradient by an approximate order of magnitude to 2 ng mL^{-1} mm^{-1}. The VEGF concentrations for the sink and source channels were chosen to yield average absolute concentrations equal to that within zone 1 and zone 4 of the previous experiments, 20 and 30 ng mL^{-1}, respectively. At both low and high absolute VEGF concentrations, the shallow 2 ng mL^{-1} mm^{-1} VEGF gradient was unable to induce HUVEC chemotaxis, Fig. 4E and F, respectively. Therefore, similar to the orientation of three-dimensional endothelial cell sprouting, two-dimensional HUVEC chemotaxis also displays a minimum threshold gradient response (~14 ng mL^{-1} mm^{-1}) that is similar in magnitude.

Filopodia extension in VEGF gradients

Endothelial cell migration requires proper rearrangement of the cellular cytoskeleton. Upon VEGF exposure, actin filaments are rapidly phosphorylated and filopodia sprouting begins to occur.[39] These finger-like structures help to attach the migrating cells to the substrate and to transfer the stress from the leading edge to the cell cytoskeleton.[40,41] It is hypothesized that an abundance of filopodia on a cell tip is indicative of an active migratory mechanism within that cell.[39] Furthermore, asymmetric filopodia sprouting around the cell perimeter may be a critical step in directing migration towards or away from a chemotactic cue. To assess these hypotheses within our system, the cytoskeletal morphology was compared between HUVEC in the presence (Fig. 5A) and absence (Fig. 5B) of various VEGF gradients. The total number of filopodia extended by HUVEC exposed to all VEGF gradients (both shallow and steep) was significantly greater than the number of filopodia counted on HUVEC without VEGF stimulation, Fig. 5C. Within the VEGF gradients, no difference in the number of filopodia was observed for cells across zones 1–4 (data not shown). Therefore, the entire range of absolute VEGF concentrations tested (18–32 ng ml^{-1}) all resulted in enhanced filopodia formation compared to no VEGF exposure.

Further analysis was performed on the cells exposed to the VEGF gradients to determine if filopodia extension was asymmetric around the cell perimeter resulting in a polarized cell morphology. The digital image of each cell was bisected through its center of mass perpendicular to the direction of the concentration gradient, separating the cell perimeter into a leading edge (0–180°) and trailing edge (180–360°) of migration. A significantly larger number of filopodia were found to occur along the HUVEC leading edge under VEGF gradients that were previously shown to induce chemotaxis (gradient = 14 ng mL^{-1} mm^{-1}), Fig. 5D.

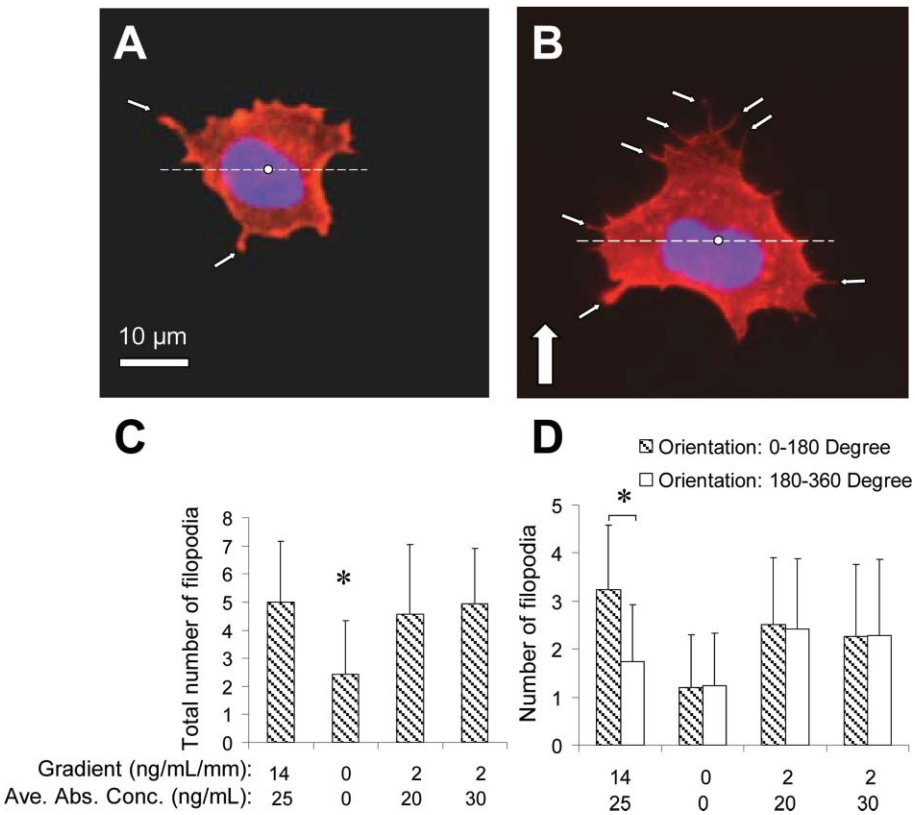

Fig. 5 HUVEC filopodia extension. (A, B) Representative fluorescent micrographs of HUVEC in the presence (A) or absence (B) of a VEGF gradient, 14 ng mL^{-1} mm^{-1}. Nuclei shown in blue and actin cytoskeleton in red. Direction of VEGF gradient is shown by the thick white arrow. Each cell is bisected into two zones (dashed line) through the center of mass (white circle). Filopodia with length >3 μm and width <1 μm are indicated by fine white arrows. (C) Total number of filopodia in cells subjected to various VEGF concentration profiles. (D) Filopodia orientation in cells subjected to various VEGF concentration profiles. Cells are bisected as shown in panels A and B; 0–180° = higher VEGF concentration, 180–360° = lower VEGF concentration. Data represent averages of n >70 cells ± standard deviation. *Statistically significant, $p < 0.001$.

In contrast, filopodia were uniformly distributed around the perimeter of HUVEC without VEGF stimulation or with VEGF gradients too shallow to induce chemotaxis (gradient = 2 ng mL^{-1} mm^{-1}). Therefore, cell polarization due to asymmetric filopodia sprouting was observed to correlate with VEGF chemotaxis. In addition, the nuclei of chemotaxing cells were often located near the trailing edge of the cell perimeter, as opposed to the center of the cytoplasm in non-chemotaxing cells, Fig. 5A, B. Taken together, these observations demonstrate that HUVEC across a range of VEGF concentrations and gradients display an actively migrating morphology with enhanced numbers of filopodia extensions. However, a minimum gradient steepness (~14 ng mL^{-1} mm^{-1}) is required to localize these filopodia along the cell perimeter, resulting in cell polarization and directed migration. These findings suggest that a change in VEGF concentration across the surface of a single cell (rather than the absolute VEGF concentration) stimulates filopodia localization, and the direction of filopodia extension correlates with the direction of chemotactic migration. These results further suggest that there may be two separate requirements for a VEGF concentration profile to induce HUVEC chemotaxis. First, the absolute concentration must be sufficient to increase filopodia extension. Second, the concentration gradient must be steep enough to induce filopodia localization and cell polarization.

Conclusion

In this study, we report the design and validation of a simple microfluidic device capable of producing a stable concentration gradient within a cell culture chamber. The principles guiding this design are similar to other gradient generators that rely solely on Fickian diffusion to establish the concentration gradient;[8–16] however, our design has the additional combined advantages of producing a constant gradient at equilibrium (allowing study of cellular phenomena across hours and days), a simple, one-step PDMS fabrication without requiring additional components such as membranes or hydrogels, and a large cell culture area (1 mm × 4 mm) to allow visualization of multiple migrating cells in both two-and three-dimensions. Because this microfluidic design operates at steady-state, the device is capable of producing a stable, quantifiable concentration gradient in the cell culture chamber for an indefinite length of time. The design also restricts fluid convection into the cell culture chamber, making the device ideal for studies of shear-sensitive cell types such as endothelial cells and non-adherent cells. This simple device may also be used to study the effects of autocrine and paracrine cell signalling inside the cell culture chamber[10] as well as the study of three-dimensional migration through hydrogels loaded into the cell culture chamber, thus mimicking the *in vivo*

cellular environment. In addition, due to the simple fabrication process, the device can be easily altered to produce an array of competing concentration gradients to study the potential competition or synergy between multiple factors. Therefore, this microfluidic device is expected to be widely applicable to the quantitative study of a range of cell biology questions.

As validation of the microfluidic device, HUVEC polarization and chemotaxis in response to VEGF stimulation was studied quantitatively. HUVEC migration towards higher VEGF concentrations occurred within a 14 ng mL^{-1} mm^{-1} gradient but was absent from a 2 ng mL^{-1} mm^{-1} gradient at similar VEGF absolute concentrations. This suggests that the slope of the concentration gradient is an important criterion in inducing chemotaxis. HUVEC exposed to VEGF gradients with an absolute concentration of at least 20 ng mL^{-1} displayed higher numbers of filopodia than cells without VEGF stimulation. Along the leading edge of chemotaxing HUVEC, localization of filopodia was observed. These results suggest that the presence of a VEGF concentration gradient across the surface of a single cell, rather than the absolute VEGF concentration, induces HUVEC polarization, while the absolute VEGF concentration enhances the overall number of filopodia extensions. Therefore, the VEGF concentration profile requirements to induce HUVEC chemotaxis may be two-fold: first, the absolute concentration must be sufficient to stimulate enhanced filopodia formation, and second, the concentration gradient must be steep enough to induce filopodia localization, cell polarization, and subsequent directed migration. Ongoing studies will utilize a single cell tracking system to follow an individual cell's path during chemotaxis to further test these hypotheses across a wider range of absolute concentrations and concentration gradients. These studies will allow quantification of the minimum absolute concentration and minimum concentration gradient required to induce polarization and chemotaxis as well as measurement of the average cell migration speed and cytoskeletal rearrangement over time. We are especially interested in determining if the increased number of filopodia displayed by cells under conditions with high VEGF concentrations but gradients below the minimum chemotaxis threshold have an increased random migration speed compared to non-stimulated cells. These studies are expected to yield new insights into the amplification mechanism underlying VEGF signalling and subsequent endothelial cell polarization and chemotaxis, a process critical to angiogenesis.

Acknowledgements

We thank the Stanford Microfluidic Foundry for help with device fabrication and NIH for financial support.

References

1 P. J. Hung, P. J. Lee, P. Sabounchi, N. Aghdam, R. Lin and L. P. Lee, *Lab Chip*, 2005, **5**, 44–48.
2 L. G. Griffith and M. A. Swartz, *Nat. Rev. Mol. Cell Biol.*, 2006, **7**, 211–224.
3 S. K. Dertinger, D. T. Chiu, N. L. Jeon and G. M. Whitesides, *Anal. Chem.*, 2001, **73**, 1240–1246.
4 B. G. Chung, L. A. Flanagan, S. W. Rhee, P. H. Schwartz, A. P. Lee, E. S. Monuki and N. L. Jeon, *Lab Chip*, 2005, **5**, 401–406.
5 F. Lin, C. M. C. Nguyen, S. J. Wang, W. Saadi, S. P. Gross and N. L. Jeon, *Ann. Biomed. Eng.*, 2005, **33**, 475–482.
6 S. Li, *Methods Mol. Biol.*, 2005, **294**, 107–121.
7 G. M. Walker, J. Sai, A. Richmond, M. Stremler, C. Y. Chung and J. P. Wikswo, *Lab Chip*, 2005, **5**, 611–618.
8 S. Cheng, S. Heilman, M. Wasserman, S. Archer, M. L. Shuler and M. Wu, *Lab Chip*, 2007, **7**, 763–769.
9 J. Diao, L. Young, S. Kim, E. A. Fogarty, S. M. Heilman, P. Zhou, M. L. Shuler, M. Wu and M. P. DeLisa, *Lab Chip*, 2006, **6**, 381–388.
10 V. V. Abhyankar, M. A. Lokuta, A. Huttenlocher and D. J. Beebe, *Lab Chip*, 2006, **6**, 389–393.
11 C. H. Hsu and A. Folch, *Appl. Phys. Lett.*, 2006, **89**, 144102.
12 T. M. Keenan, C. H. Hsu and A. Folch, *Appl. Phys. Lett.*, 2006, **89**, 114103.
13 B. G. Chung, F. Lin and N. L. Jeon, *Lab Chip*, 2006, **6**, 764–768.
14 D. Irimia, G. Charras, N. Agrawal, T. Mitchison and M. Toner, *Lab Chip*, 2007, **7**, 1783–1790.
15 W. Saadi, S. W. Rhee, F. Lin, B. Vahidi, B. G. Chung and N. L. Jeon, *Biomed. Microdevices*, 2007, **9**, 627–635.
16 H. Wu, B. Huang and R. N. Zare, *J. Am. Chem. Soc.*, 2006, **128**, 4194–4195.
17 L. Lamalice, F. L. Boeuf and J. Huot, *Circ. Res.*, 2007, **100**, 782–794.
18 K. A. Hotchkiss, A. W. Ashton, R. S. Klein, M. L. Lenzi, G. Hui Zhu and E. L. Schwartz, *Cancer Res.*, 2003, **63**, 527–533.
19 G. Ahrendt, D. E. Chickering and J. P. Ranieri, *Tissue Eng.*, 1998, **4**, 117–130.
20 A. Hoeben, B. Landuyt, M. S. Highley, H. Wildiers, A. T. Van Oosterom and E. A. De Bruijn, *Pharmacol. Rev.*, 2004, **56**, 549–580.
21 P. A. Dimilla, J. A. Quinn, D. A. Lauffenburger and S. M. Albelda, *Matrix*, 1990, **10**, 223.
22 Y. Wang, J. Chang, K. Chen, S. Li, J. Y.-S. Li, C. Wu and S. Chien, *Am. J. Physiol. Heart Circ. Physiol.*, 2007, **104**, 8875–8879.
23 S. Hsu, R. Thakar, D. Liepmann and S. Li, *Biochem. Biophys. Res. Commun.*, 2005, **337**, 401–409.
24 B. P. Eliceiri, *Circ. Res.*, 2001, **89**, 1104–1110.
25 K. C. Boardman and M. A. Swartz, *Circ. Res.*, 2003, **92**, 801–808.
26 C. L. E. Helm, M. E. Fleury, A. H. Zisch, F. Boschetti and M. A. Swartz, *Proc. Natl. Acad. Sci. U. S. A.*, 2005, **102**, 15779–15784.
27 E. A. Silva and D. J. Mooney, *J. Thromb. Haemostasis*, 2007, **5**, 590–598.
28 D. F. Lazarous, M. Shou, M. Scheinowitz, E. Hodge, V. Thirumurti, A. N. Kitsiou, J. A. Stiber, A. D. Lobo, S. Hunsberger and E. Guetta *et al.*, *Circulation*, 1996, **94**, 1074–1082.
29 D. I. Leavesley, M. A. Schwartz, M. Rosenfeld and D. A. Cheresh, *J. Cell Biol.*, 1993, **121**, 163–170.
30 C. E. Semino, R. D. Kamm and D. A. Lauffenburger, *Exp. Cell Res.*, 2006, **312**, 289–298.
31 S. H. Zigmond, *J. Cell Biol.*, 1977, **75**, 606–616.
32 D. Zicha, G. A. Dunn and A. F. Brown, *J. Cell Sci.*, 1991, **99**, 769–775.
33 R. R. Chen, E. A. Silva, W. W. Yuen, A. A. Brock, C. Fischbach, A. S. Lin, R. E. Guldberg and D. J. Mooney, *FASEB J.*, 2007, **21**, 3896–3903.
34 F. Mac Gabhann and A. S. Popel, *Am. J. Physiol. Heart Circ. Physiol.*, 2005, **288**, H2851–H2860.
35 F. M. White, *Viscous Fluid Flow*, McGraw-Hill, 2nd edn, 1991.
36 F. Lin and E. C. Butcher, *Lab Chip*, 2006, **6**, 1462–1469.
37 T. V. Byzova, C. K. Goldman, N. Pampori, K. A. Thomas, A. Bett, S. J. Shattil and E. F. Plow, *Mol. Cell*, 2000, **6**, 851–860.
38 R. O. Hynes and B. L. Bader, *Thromb. Haemostasis*, 1997, **78**, 83–87.
39 H. Gerhardt, M. Golding, M. Fruttiger, C. Ruhrberg and A. Lundkvist, *J. Cell Biol.*, 2003, **161**, 1163–1177.
40 M. Clauss and G. Breier, *Mechanisms of angiogenesis*, Birkhauser, 2005.
41 A. J. Ridley, M. A. Schwartz, K. Burridge, R. A. Firtel, M. H. Ginsberg, G. Borisy, J. T. Parsons and A. R. Horwitz, *Science*, 2003, **302**, 1704–1709.